Nonlinear Dyn (2018) 93:1109–1120
https://doi.org/10.1007/s11071-018-4248-4

ORIGINAL PAPER

Robust adaptive dynamic surface control for hypersonic vehicles

Naibao He · Qian Gao · Hector Gutierrez · Changsheng Jiang · Yifei Yang · Yuchun Bi

Received: 9 April 2017 / Accepted: 29 March 2018 / Published online: 12 April 2018

Abstract An adaptive dynamic surface control (DSC) scheme is proposed for the multi-input multi-output attitude control of near-space hypersonic vehicles (NHV). The proposed control strategy can improve the control performance of NHV despite uncertainties and external disturbances. The proposed controller combines dynamic surface control and radial basis function neural network (RBFNN) and is designed to control the longitudinal dynamics of NHV. The DSC technique is used to handle the problem of "explosion of complexity" inherent to the conventional backstepping method. RBFNN is used to approximate the unknown nonlinear function, and a robustness component is introduced in the controller to cancel the influence of compound disturbance and improve robustness and adaptation of the system. Simulation results show that the proposed strategy possesses good robustness and fast response.

N. He (✉) · Y. Yang · Y. Bi
School of Electrical and Information Engineering, Jiangsu University of Technology, Changzhou, China
e-mail: henaibao@126.com

N. He · H. Gutierrez
Mechanical and Aerospace Engineering, Florida Institute of Technology, Melbourne, FL, USA
e-mail: hgutier@fit.edu

Q. Gao
School of Computer Engineering, Jiangsu University of Technology, Changzhou, China

C. Jiang
College of Automatic Engineering, Nanjing University of Aeronautics and Astronautics, Nanjing, China

Keywords Dynamic surface control · Near-space hypersonic vehicles · Robust control · Radial basis function neural network

List of symbols

α	The angle of attack (rad)
β	The side slip angle and the roll angle (rad)
γ	The flight path angle (rad)
C_{D}	Drag coefficient
C_{L}	Lift coefficient
C_{T}	Thrust coefficient
D	Drag (lbf)
H	The altitude (ft)
I_{yy}	Moment of inertia (slug ft^2)
L	Lift (lbf)
M_{yy}	Pitching moment (lbf ft)
M	Mass (slug)
μ	The angle of bank (rad)
q	The pitch rate (rad/s)
$\bar{r}$	Radial distance from Earth's center (ft)
T	Thrust (lbf)
V	The velocity (ft/s)
r	The yaw rate (rad/s)
p	The roll rate (rad/s)

1 Introduction

The near-space hypersonic vehicle (NHV) is a novel aerospace aircraft with an important role in military and

civil applications due to lower launch cost, maintainability, speed of redeployment and reusability. Effective control of the NHV remains a critical challenge of the system's design: the near-space hypersonic vehicle dynamics are severely nonlinear, time-varying, highly uncertain, strongly coupled, and suffers external disturbances from changes in the fight environment, propulsion system perturbation, atmospheric turbulence, wind gust, friction disturbances and others. Robust design of the NHV flight controller is a challenging problem [1–7]. A near-space hypersonic vehicle model cannot be accurately determined and the aerodynamic pressure, aerodynamic heating, and thermoelastic dynamics are difficult to precisely measure or estimate in such environment. For example, in the second flight of HTV-2 in 2011, the investigation from the Engineering Review Board (ERB) found that larger than anticipated portions of the vehicle's skin peeled from the aerostructure, and the resulting gaps created strong, impulsive shock waves around the vehicle as it travelled at nearly 13,000 miles per hour, causing the vehicle to roll abruptly. The severity of the continued disturbances finally exceeded the vehicle's ability to recover [8].

Recently, the NHV technique is more attentions to address this problem. Various control strategies have been proposed. In [1], an adaptive neural tracking control scheme was developed for the NHV with stochastic disturbances. In [9], an NDI-based L1 adaptive control scheme was designed for a generic hypersonic vehicle model with input gain uncertainty and input disturbances. In [10], second-order fast terminal sliding mode control design based on LMI for a class of nonlinear uncertain systems and its application to chaotic systems. A variable domain fuzzy control approach for the NHV was present in [11]. Xu et al. designed a multi-input/multi-output adaptive sliding controller for the longitudinal dynamics of a generic hypersonic vehicle [12]. In [13], an adaptive dynamic surface control (DSC) scheme was proposed for the NHV with input saturation using a Nussbaum disturbance observer. In [14], robust flight control schemes were introduced for the hypersonic vehicle with uncertainties and external disturbances using a disturbance observer and neural networks. Jiang et al. [15] addressed the problem of integrated robust fault estimation and accommodation in discrete-time T–S fuzzy systems. Fu et al. [16] investigated the sliding mode control with unidirectional auxiliary surfaces for the NHV. A second-order dynamic terminal sliding mode control scheme was proposed for the hypersonic vehicle in [17]. Du et al. [18] presented the functional link network (FLN) control method for the NHV with dynamic thrust and parametric uncertainties. Wang et al. [19] proposed a novel T–S fuzzy tracking control method for the reentry attitude tracking problem of a reusable launch vehicle. Feedback linearization has been used for controller design of the NHV with uncertain parameters and input constraints [20]. Saleh et al. [21,22] presented a novel adaptive global nonlinear sliding surface for a class of disturbed nonlinear dynamical systems. In [23], an adaptive super-twisting global nonlinear sliding mode tracker control was developed for n-link rigid robotic manipulators. It is safe to say that robust flight control of the NHV is a challenging problem.

In the control strategies, mentioned above backstepping control has been an important tool for nonlinear system analysis and control. Several applications of the backstepping method have been presented over the past few decades [24,27]. However, due to the repeated differentiation of virtual controls, the backstepping approach suffers from "strict-feedback" and "explosion of complexity" issues [28,29]. Strict-feedback form means that the ith dynamic equation of a system with dimension n can only be dependent on the state variables x_1 to x_{i+1}, and the state variable x_{i+1} serves as an input only in the ith dynamic equation [28]. Furthermore, in backstepping control one has to compute several time derivatives of virtual inputs to design the controller. The number of time derivatives increases with the dimensions of the plant to be controlled: this is called "explosion of complexity", which is caused by the successive differentiation of certain nonlinear functions.

In this paper, the dynamic surface control method is used to handle the "explosion of complexity" by incorporating a first-order filter of the synthetic virtual control input in flight control, and the adaptive controller is constructed by combining the dynamic surface control technique with a robustness item. This addresses controller design issues related to both parametric model uncertainty and external disturbances.

The main contributions of the proposed method relative to the state of the art are:

(1) An adaptive robust backstepping controller design is proposed for the near-space hypersonic vehicle, in the presence of time-varying uncertainties and external disturbances.

(2) To eliminate differentiation of the virtual control laws, an adaptive dynamic surface control scheme is used for the control of the longitudinal dynamics. This has also been applied to the tracking control of the attitude angle of the NHV.
(3) A radial basis function neural network is used to approximate the unknown compound disturbance, while a robustness item is introduced into the virtual controller to cancel the influence of the compound disturbance and improve robustness and adaptation of the overall system.

The paper is organized as follows: In Sect. 2, a mathematical model of the longitudinal dynamics of the NHV is derived, and the input/output feedback linearization is stated. Section 3 describes the robust controller design of the longitudinal dynamics of the NHV and the design of the dynamic surface controller combining the radial basis function neural network and robustness item. The stability analysis is in Sect. 4. Simulation results that illustrate the effectiveness of the proposed approach are presented in Sect. 5 and the conclusion is in Sect. 6.

2 Problem formulation

2.1 Mathematical model of the NHV

The model adopted in the paper was developed by NASA Langley Research Center [11]. The longitudinal dynamics of the NHV are given by the following model:

$$\dot{V} = \frac{T\cos\alpha - D}{M} - \frac{\mu\sin\gamma}{\bar{r}^2} \tag{1}$$

$$\dot{\gamma} = \frac{L + T\sin\alpha}{MV} - \frac{(\mu - V^2\bar{r})\cos\gamma}{V\bar{r}^2} \tag{2}$$

$$\dot{H} = -\dot{z} = V\sin\gamma \tag{3}$$

$$\dot{\alpha} = q - \dot{\gamma} \tag{4}$$

$$\dot{q} = \frac{M_{yy}}{I_{yy}} \tag{5}$$

where $T = \hat{q}SC_{\mathrm{T}}$, $D = \hat{q}SC_{\mathrm{D}}$, $L = \hat{q}SC_{\mathrm{L}}$, $M_{yy} = \hat{q}\bar{c}[C_M(\alpha) + C_M(\delta_e) + C_M(q)]$, V is the velocity, γ the flight path angle, H the altitude, α the angle of attack, and q the pitch rate.

2.2 Input/output linearization

Input/output feedback linearization is an important method used in nonlinear control, subject to satisfying the relative degree condition. In this method, nonlinear MIMO systems can be transformed into linear form by using Lie derivatives to define a nonlinear coordinate transformation that renders the system linear:

$$\begin{cases} \dot{\boldsymbol{x}} = \boldsymbol{f}(\boldsymbol{x}) + \sum_{i=1}^{m} \boldsymbol{g}_i(\boldsymbol{x})\boldsymbol{u}_i \\ y_1 = h_1(\boldsymbol{x}) \\ \vdots \\ y_m = h_m(\boldsymbol{x}) \end{cases} \tag{6}$$

where $\boldsymbol{f}(\boldsymbol{x})$, $\boldsymbol{g}(\boldsymbol{x})$, and $h(\boldsymbol{x})$ are sufficiently smooth functions. For the input/output linearization transformation, the Lie derivative can be expressed as

$$y_i^{(r_i)} = L_f^{r_i}(h_i) + \sum_{k=1}^{m} L_{g_k}[L_f^{r_i-1}(h_i)]u_k \tag{7}$$

where r_i is the relative degree. If r_i satisfies the following condition:

$$r_1 + r_2 + \cdots + r_m \le n \tag{8}$$

the nonlinear system (6) can only be partially linearized. For NHVs, the linearized model is developed by repeated differentiation of V and H as follows:

$$\begin{cases} \dot{V} = \frac{T\cos\alpha - D}{M} - \frac{\mu\sin\gamma}{\bar{r}^2} \\ \ddot{V} = \frac{1}{M}W_1^T\dot{x} \\ V^{(3)} = \frac{1}{M}\left(W_1^T\ddot{x} + \dot{x}^T\boldsymbol{\Omega}_2\dot{x}\right) \end{cases} \tag{9}$$

$$\begin{cases} \dot{H} = V\sin\gamma \\ \ddot{H} = \dot{V}\sin\gamma + V\dot{\gamma}\cos\gamma \\ H^{(3)} = \ddot{V}\sin\gamma + 2\dot{V}\dot{\gamma}\cos\gamma - V\dot{\gamma}^2\sin\gamma + V\ddot{\gamma}\cos\gamma \\ H^{(4)} = V^{(3)}\sin\gamma + V\gamma^{(3)}\cos\gamma + 3\ddot{V}\dot{\gamma}\cos\gamma \\ \qquad -3\dot{V}\dot{\gamma}^2\sin\gamma + 3\dot{V}\ddot{\gamma}\cos\gamma \\ \qquad -3V\dot{\gamma}\ddot{\gamma}\sin\gamma - V\dot{\gamma}^3\cos\gamma \end{cases} \tag{10}$$

where $x = \left[V\ \gamma\ \alpha\ \lambda\ H\right]^T$, $\ddot{\gamma} = \pi_1^T\dot{x}$, $\gamma^{(3)} = \pi_1^T\ddot{x} + \dot{x}^T\Pi_2\dot{x}$. Then

$$\begin{cases} \dot{x}_1 = x_2 \\ \dot{x}_2 = x_3 \\ \dot{x}_3 = f + Gu \end{cases} \tag{11}$$

where $x_1 = h(x) = \left[V\ \dot{H}\right]^T$, $x_2 = \left[\dot{V}\ \ddot{H}\right]^T$, $x_3 = \left[V_0^{(3)}\ H_0^{(4)}\right]^T$, $f = \left[V_0^{(3)}\ H_0^{(4)}\right]^T$, $G = \begin{bmatrix} b_{11} & b_{12} & b_{13} \\ b_{21} & b_{22} & b_{23} \end{bmatrix}$, $u = [\lambda_{com}\ \delta_e\ \delta_a]^T$ The detailed expressions for W_1, Ω_2 and Π_2 are given in "Appendix".

3 Design of the NHV dynamic surface control

Due to the complexity of the flight environment, such as time-varying strong airflow, its effect on rudders, actuators, and other fuselage components, etc., the uncertainties and external disturbances must be considered in controller design.

Consider the hypersonic vehicle dynamic longitudinal model (12),

$$\begin{cases} \dot{x}_1 = x_2 + \Delta_1(\bar{x}_1, t) \\ \dot{x}_2 = x_3 + \Delta_2(\bar{x}_2, t) \\ \dot{x}_3 = f(\bar{x}_3) + G(\bar{x}_3)u + \Delta_3(\bar{x}_3, t) \end{cases} \tag{12}$$

$\Delta_i(\bar{x}_i, t)$ are the compounded disturbances, which includes the uncertainty and external disturbances.

In this paper, the control objective is to select a vector that forces the velocity V and altitude H to track a desired command $y_r(t) = \left[V_r(t)\, \dot{H}_r(t)\right]^T, t \geq 0$. To design the adaptive DSC for the system given by Eq. (12), the following assumptions and lemmas are required:

Assumption 1 For the parameter perturbation and external disturbance $\Delta_i(\bar{x}_i, t)$, there exist unknown positive constants D_i, such that $\|\Delta_i(\bar{x}_i, t)\| \leq D_i$ (i = 1, 2, …, m).

Since RBFNN can provide a good approximation function to an arbitrary accuracy, it is here proposed to approximate the nonlinear unknown continuous function $\Delta_i(\bar{x}_i, t)$.

The RBFNN is defined as follows:

$$u = W^T \varphi(X, \bar{\mu}, \sigma) \tag{13}$$

Where $X \in \Omega_X \in R^N$ is the input to the neural network, $\bar{\mu}$ is the center of the Gaussian basis function, $\bar{\mu} = \left[\bar{\mu}_1^T, \cdots, \bar{\mu}_l^T\right]^T$, σ_i is the width of the Gaussian basis function $\sigma = [\sigma_1, \cdots, \sigma_l]^T$, and $\varphi = [\varphi_i]_{l\times 1}$ is the Gaussian basis function:

$$\varphi_i(X, \bar{\mu}, \sigma) = \exp\left[\frac{-(X - \bar{\mu}_i)^T (X - \bar{\mu}_i)}{\sigma_i^2}\right] \tag{14}$$

$i = 1, \cdots, l$.

The neural network defined above can approximate any continuous function with arbitrary precision on the compact set Ω_X, therefore:

$$\Delta(X) = W^{*T} \varphi^*\left(X, \bar{\mu}^*, \sigma^*\right) + \varepsilon(X) \tag{15}$$

where $\varepsilon(X)$ denotes the approximation error of the neural network and satisfies $\varepsilon_H > 0$.

Assumption 2 For the input $X \in \Omega_X$, there exists an optimal constant weight W^*, $\|\varepsilon(X)\| \leq \varepsilon_H$, such that $\|W^*\|_F \leq \bar{W}$, where $\bar{W} > 0$.

In this section, the backstepping control is presented. The DSC design procedure includes three steps to yield the control law u. The design procedure is as follows:

Step 1 Considering Eq. (12):

$$\dot{x}_1 = x_2 + \Delta_1(\bar{x}_1, t)$$

We define

$$w_1 = x_1 - y_r \tag{16}$$

where $\boldsymbol{y}_r$ is the reference command. The time derivative of Eq. (16) is

$$\dot{w}_1 = x_2 + \Delta_1(\bar{x}_1, t) - \dot{y}_r \tag{17}$$

For Eq. (17), there exists an ideal control law x_2^*

$$x_2^* = -(-\dot{y}_r + k_1 w_1 + W^{*T}_1 \varphi_1(\bar{x}_1) + \boldsymbol{\varepsilon}_1) \tag{18}$$

where $k_1 > 0$ is a design parameter, $\hat{W}_1$ is the estimated value of W_1^*, and $\tilde{W}_1 = \hat{W}_1 - W_1^*$ is the weight estimation error. Since x_2^* is not available, the actual virtual controller x_{2d} is

$$x_{2d} = -(-\dot{y}_r + k_1 w_1 + \hat{W}_1^T \varphi_1(\bar{x}_1) + v_1) \tag{19}$$

where v_1 is a robust term and is defined as

$$v_1 = \frac{w_1 \varepsilon_{1H}}{\|w_1\| + 1} \tag{20}$$

The adaptive law of $\hat{W}_1$ is designed as

$$\dot{\hat{W}}_1 = \dot{\hat{W}}_1 = \Gamma_1 \varphi_1(\bar{x}_1) w_1^T - \eta_1 \Gamma_1 \hat{W}_1 \tag{21}$$

where $\eta_1 > 0$ is the design parameter, and $\Gamma_1 = \Gamma_1^T > 0$ is the constant matrix to be designed. In the conventional backstepping method, the tracking error is defined as:

$$w_2 = x_2 - z_2 \tag{22}$$

which yields:

$$\dot{w}_2 = x_3 + \Delta_2(\bar{x}_2, t) - \dot{z}_2 \tag{23}$$

The second subsystem of the virtual control law is obtained similarly:

$$\begin{aligned} \dot{x}_{3d} = &\frac{\partial x_{3d}}{\partial x_1^T}\dot{x}_1 + \frac{\partial x_{3d}}{\partial x_2^T}\dot{x}_2 + \frac{\partial x_{3d}}{\partial \hat{W}_1}\dot{\hat{W}}_1 + \frac{\partial x_{3d}}{\partial \hat{W}_2}\dot{\hat{W}}_2 \\ &+ \frac{\partial x_{3d}}{\partial y_r^T}\partial \dot{y}_r + \frac{\partial x_{3d}}{\partial \dot{y}_r^T}\ddot{y}_r + \frac{\partial x_{3d}}{\partial \ddot{y}_r^T} y_r^{(3)} \end{aligned} \tag{24}$$

This illustrates how the backstepping method has brought the problem of "explosion of complexity". In [30,31], it is proposed that a first-order filter is used to estimate the virtual control law, so that the conventional backstepping method can be used without derivation of the virtual control law. Therefore, before calculating the virtual control law of the second subsystem, we define the new state variable z

$$\tau_2 \dot{z}_2 + z_2 = x_{2d}\,,\ z_2(0) = x_{2d}(0) \tag{25}$$

where τ_2 is a time constant that can be used to approximate the virtual control law with the estimated value from the filter, effectively avoiding the complex calculation problem from the backstepping method.

Step 2 From the second subsystem, we have

$$\dot{w}_2 = \dot{x}_2 - \dot{z}_2 = x_3 + \Delta_2(\bar{x}_2) - \dot{z}_2$$

The ideal control law x_3^* is

$$x_3^* = -(-\dot{z}_2 + k_2 w_2 + w_1 + W_2^{*T}\varphi_2(\bar{x}_2) + \varepsilon_2) \tag{26}$$

Because we cannot get x_3^*, the virtual controller x_{3d} for x_3^* is

$$x_{3d} = -(-\dot{z}_2 + k_2 w_2 + w_1 + \hat{W}_2^T\varphi_2(\bar{x}_2) + v_2) \tag{27}$$

where $\hat{W}_2$ is the estimated value of W_2^*. The adaptive law of $\hat{W}_2$ is designed as

$$\dot{\tilde{W}}_2 = \dot{\hat{W}}_2 = \Gamma_2\varphi_2(\bar{x}_2)w_2^T - \eta_2\Gamma_2\hat{W}_2 \tag{28}$$

where $\eta_2 > 0$ is the design parameter, and $\Gamma_2 = \Gamma_2^T > 0$ is the design constant matrix. v_2 is a robustness term, defined as follows:

$$v_2 = \frac{w_2\varepsilon_{2H}}{\|w_2\| + 1} \tag{29}$$

To estimate x_{3d}, the low-order filter is designed as:

$$\tau_3\dot{z}_3 + z_3 = x_{3d}\,,\ z_3(0) = x_{3d}(0) \tag{30}$$

where τ_3 is a time constant.

Step 3 Consider the third subsystem

$$\dot{x}_3 = f(\bar{x}_3) + G(\bar{x}_3)\,u + \Delta_3(\bar{x}_3, t)$$

$$\dot{w}_3 = \dot{x}_3 - \dot{z}_3 = G(\bar{x}_3)u + f(\bar{x}_3) + \Delta_3(\bar{x}_3, t) - \dot{z}_3 \tag{31}$$

To eliminate the influence of the uncertainty $\Delta_3(\bar{x}_3, t)$, one can use:

$$\Delta_3(\bar{x}_3, t) = W_3^{*T} j_3(\bar{x}_3) + \varepsilon_3 \tag{32}$$

where $\|\varepsilon_3\| \le \varepsilon_{3H}$, $\varepsilon_{3H} > 0$, and $\bar{x}_3$ is the input to the RBF neural network. In this context, it is clearly difficult to calculate the ideal controller u^*:

$$u^* = -G(\bar{x}_3)^{-1}(f(\bar{x}_3) - \dot{z}_3 + k_3 w_3 + w_2 + W_3^{*T}\varphi_3 + \varepsilon_3) \tag{33}$$

Instead, we propose the controller u

$$u = -G(\bar{x}_3)^{-1}(f(\bar{x}_3) - \dot{z}_3 + k_3 w_3 + w_2 + \hat{W}_3^T\varphi_3 + v_3) \tag{34}$$

where $\hat{W}_3$ is the estimated value of W_3^*. The adaptive law of $\hat{W}_3$ is designed as

$$\dot{\tilde{W}}_3 = \dot{\hat{W}}_3 = \Gamma_3\varphi_3(\bar{x}_3)w_3^T - \eta_3\Gamma_3\hat{W}_3 \tag{35}$$

where $\eta_3 > 0$ is the design parameter, and $\Gamma_3 = \Gamma_3^T > 0$ is the design constant matrix. v_3 is a robustness term defined as follows:

$$v_3 = \frac{w_3\varepsilon_{3H}}{\|w_3\| + 1} \tag{36}$$

4 Stability analysis

To analyze the stability of the closed-loop system, the robust adaptive control of the hypersonic vehicle based on the dynamic surface can be shown as follows:

Theorem 1 *For the closed-loop system Eq. (12), the virtual control laws from Eqs. (19), (27), and the control law given by Eq. (34), the robust control laws are designed as Eqs. (20), (29) and (36) and the adaptive laws are designed as Eqs. (21), (28) and (35). With appropriately designed parameters k_i, $\boldsymbol{\Gamma}_i$, η_i, the system is uniformly bounded.*

Proof Consider the Lyapunov function candidate

$$L(t) = \frac{1}{2}\sum_{i=1}^{3}\left(w_i{}^T w_i + tr\left(\tilde{W}_i^T\Gamma_i{}^{-1}\tilde{W}_i\right)\right) + \frac{1}{2}\sum_{i=1}^{2} y_{i+1}^T y_{i+1} \tag{37}$$

Differentiating $L(t)$, we obtain

$$\dot{L}(t) = \sum_{i=1}^{3}\left(w_i^T\dot{w}_i + tr\left(\tilde{W}_i^T\boldsymbol{\Gamma}_i{}^{-1}\dot{\hat{W}}_i\right)\right) + \sum_{i=1}^{2} y_{i+1}^T\dot{y}_{i+1} \tag{38}$$

Using Eqs. (16), (22), and (25), it follows that

$$w_1^T \dot{w}_1 = w_1^T w_2 - k_1 w_1^T w_1 - w_1^T \tilde{W}_1^T \varphi_1(\bar{x}_1) + w_1^T y_2 + w_1^T \varepsilon_1 - w_1^T v_1$$

Due to

$$w_1^T \varepsilon_1 - w_1^T v_1 \le \|w_1\| \varepsilon_{1H} - w_1^T \frac{w_1 \varepsilon_{1H}}{\|w_1\| + 1} = \frac{\|w_1\| \varepsilon_{1H}}{\|w_1\| + 1} \le \varepsilon_{1H}$$

By Young's inequality, we have

$$w_1^T \dot{w}_1 \le (2 - k_1)\|w_1\|_2{}^2 + \frac{1}{4}\|w_2\|_2{}^2 + \frac{1}{4}\|y_2\|_2{}^2 + \varepsilon_{1H} - w_1^T \tilde{W}_1^T \varphi_1(\bar{x}_1) \tag{39}$$

□

Similarly

$$w_2^T \dot{w}_2 \le (2 - k_2)\|w_2\|_2{}^2 + \frac{1}{4}\|w_3\|_2{}^2 + \frac{1}{4}\|y_3\|_2{}^2 + \varepsilon_{2H} - w_2^T \tilde{W}_2^T \varphi_2(\bar{x}_2) \tag{40}$$

and

$$w_3^T \dot{w}_3 \le -k_3\|w_3\|_2{}^2 + \varepsilon_{3H} - w_3^T \tilde{W}_3^T \varphi_3(\bar{x}_3) \tag{41}$$

The system's boundary error is described as

$$y_{i+1} = z_{i+1} - x_{(i+1)d} \tag{42}$$

according to the first-order filter

$$\tau_{i+1}\dot{z}_{i+1} + z_{i+1} = x_{(i+1)d}, \quad z_{i+1}(0) = x_{(i+1)d}(0) \tag{43}$$

we have

$$\dot{z}_{i+1} = -\frac{y_{i+1}}{\tau_{i+1}}, i = 1, ..., n-1 \tag{44}$$

then

$$\dot{y}_2 = \dot{z}_2 - \dot{x}_{2d} = \dot{z}_2 + k_1 \dot{w}_1 + \dot{\hat{W}}_1^T \varphi_1(\bar{x}_1) + \hat{W}_1^T \frac{\partial \varphi_1(\bar{x}_1)}{\partial \bar{x}_1} - \ddot{y}_r + \dot{v}_1 = -\frac{y_2}{\tau_2} + B_2(w_1, w_2, y_2, \hat{W}_1, y_r, \dot{y}_r, \ddot{y}_r) \tag{45}$$

where $B_2(w_1, w_2, y_2, \hat{W}_1, y_r, \dot{y}_r, \ddot{y}_r)$ is a continuous function. Therefore:

$$y_2^T \dot{y}_2 \le -\frac{{y_2}^T y_2}{\tau_2} + B_2\|y_2\|_2 \le -\frac{{y_2}^T y_2}{\tau_2} + \|y_2\|_2^2 + \frac{1}{4}{B_2}^2 \tag{46}$$

Similarly,

$$y_3^T \dot{y}_3 \le -\frac{{y_3}^T y_3}{\tau_3} + B_3\|y_3\|_2 \le -\frac{{y_3}^T y_3}{\tau_3} + \|y_3\|_2^2 + \frac{1}{4}{B_3}^2 \tag{47}$$

From Eq. (38) we obtain:

$$\begin{aligned}
\dot{L}(t) \le\ & (2 - k_1)\|w_1\|_2{}^2 + \frac{1}{4}\|w_2\|_2{}^2 + \frac{1}{4}\|y_2\|_2{}^2 + \varepsilon_{1H} \\
& - w_1^T \tilde{W}_1^T \varphi_1(\bar{x}_1) + (2 - k_2)\|w_2\|_2{}^2 \\
& + \frac{1}{4}\|w_3\|_2{}^2 \\
& + \frac{1}{4}\|y_3\|_2{}^2 + \varepsilon_{2H} - w_2^T \tilde{W}_2^T \varphi_2(\bar{x}_1) - k_3||w_3||_2^2 \\
& + \varepsilon_{3H} - w_3^T \tilde{W}_3^T \varphi_3(\bar{x}_3) \\
& + \sum_{i=1}^{3} tr\left(\tilde{W}_i^T \boldsymbol{\Gamma}_i{}^{-1} \dot{\hat{W}}_i\right) \\
& + \sum_{i=1}^{2} y_{i+1}^T \dot{y}_{i+1} \\
=\ & (2 - k_1)\|w_1\|_2^2 + (2\frac{1}{4} - k_2)\|w_2\|_2^2 \\
& + (\frac{1}{4} - k_3)\|w_3\|_2^2 \\
& + \sum_{i=1}^{3} \varepsilon_{iH} + \sum_{i=1}^{3} tr(-\eta_i \tilde{W}_i^T \hat{W}_i) \\
& + \sum_{i=1}^{2} (-\frac{\|y_{i+1}\|_2{}^2}{\tau_{i+1}} + 1\frac{1}{4}\|y_{i+1}\|_2{}^2 + \frac{1}{4}B_{i+1}^2)
\end{aligned}$$

where $k_1 = 2 + \alpha_0$, $k_2 = 2\frac{1}{4} + \alpha_0$, $k_3 = \frac{1}{4} + \alpha_0$, $\frac{1}{\tau_{i+1}} = 1\frac{1}{4} + \alpha_0$, $\alpha_0 = \min_{i=1,2,3}\left(\frac{\eta_i}{2\lambda_{\max}(\Gamma_i^{-1})}\right)$, and α_0 is a positive real number.

$$\begin{aligned}
\dot{L}(t) &\le \sum_{i=1}^{3}\left(-\alpha_0\|w_i\|_2^2 + \sum_{i=1}^{3} tr(-\eta_i \tilde{W}_i^T \hat{W}_i)\right) + \sum_{i=1}^{3}\varepsilon_{iH} + \sum_{i=1}^{2}\left(-\frac{\|y_{i+1}\|_2{}^2}{\tau_{i+1}} + 1\frac{1}{4}\|y_{i+1}\|_2{}^2 + \frac{1}{4}B_{i+1}^2\right) \\
&\le \sum_{i=1}^{3}\left(-\alpha_0\|w_i\|_2^2 - \frac{1}{2}\eta_i tr(\tilde{W}_i^T \tilde{W}_i)\right) + \sum_{i=1}^{3}\left(\varepsilon_{iH} + \frac{1}{2}\eta_i||W_i^*||_F^2\right)
\end{aligned}$$

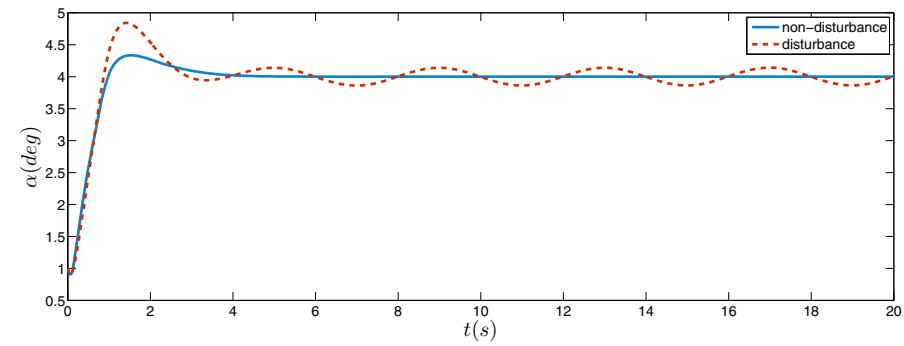

(a)

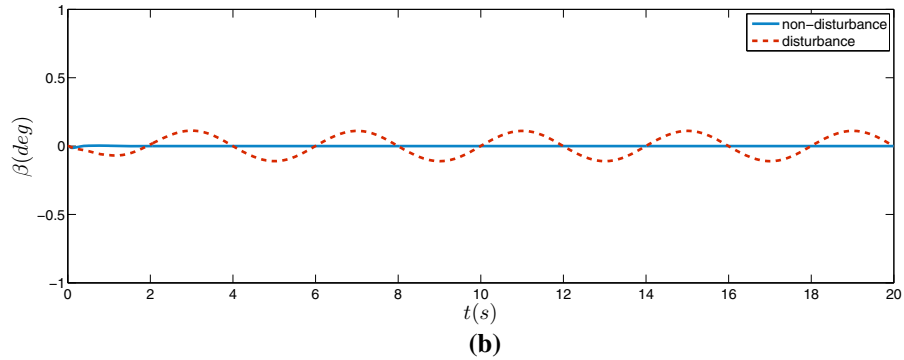

(b)

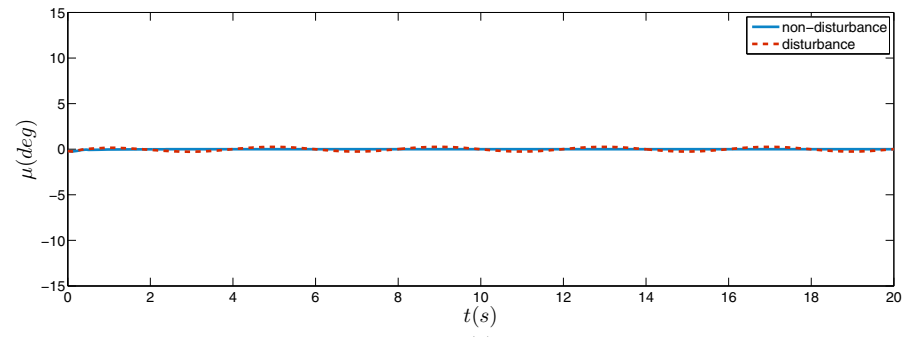

(c)

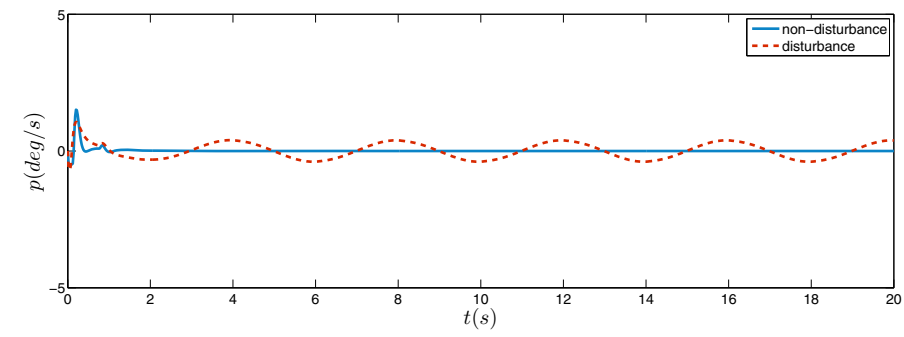

(d)

Fig. 1 Response curves of the NHV under adaptive DSC controller. **a** The attack angle α curve. **b** The sideslip angle β curve. **c** The bank angle μ curve. **d** The roll rate p curve. **e** The pitch rate q curve. **f** The yaw rate r curve

Fig. 1 continued

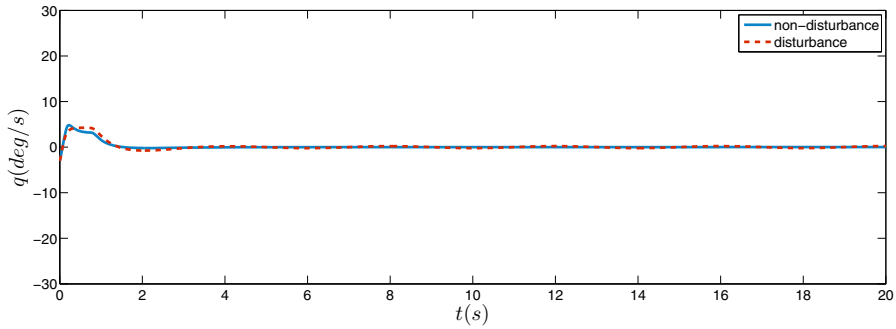

(e)

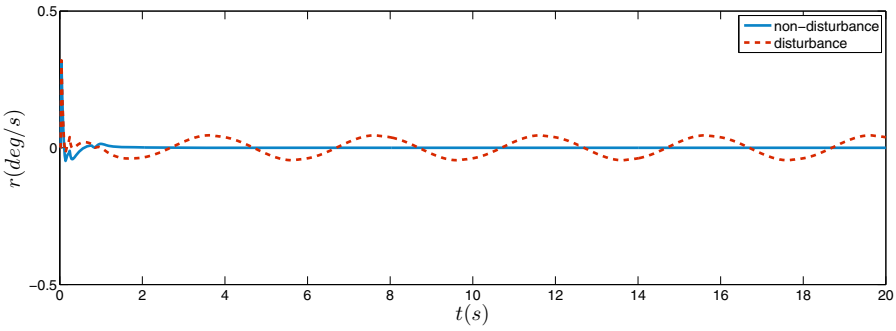

(f)

$$+\sum_{i=1}^{2}\left(-\frac{\left\|y_{i+1}\right\|_2^{\,2}}{\tau_{i+1}}+1\frac{1}{4}\left\|y_{i+1}\right\|_2^{\,2}+\frac{1}{4}B_{i+1}^2\right)$$
$$\leq -2\alpha_0 L(t)+\sum_{i=1}^{3}\left(\varepsilon_{iH}+\frac{1}{2}\eta_i||W_i^*||_F^2\right)$$
$$+\sum_{i=1}^{2}\left(\frac{1}{4}B_{i+1}^2\right) \tag{48}$$

Let $\rho=\sum_{i=1}^{3}\left(\varepsilon_{1H}+\frac{1}{2}\eta_i||W_i^*||_F^2\right)+\sum_{i=1}^{2}\left(\frac{1}{4}B_{i+1}^2\right)$

Then

$$\dot{L}(t)\leq -2\alpha_0 L(t)+\rho \tag{49}$$

□

which completes the proof.

Note In Theorem 1, the tracking error converges to a residual set that can be made arbitrarily small by properly choosing the design parameters. In the next step, we will prove each subsystem is stable.

Select the Lyapunov function of the first subsystem:

$$V_1=\frac{{w_1}^T w_1}{2}+\frac{1}{2}tr\left[\tilde{W}_1^T\Gamma^{-1}{}_1\tilde{W}_1\right] \tag{50}$$

Taking the time derivative of V_1

$$\dot{V}_1={w_1}^T\dot{w}_1+tr\left[\tilde{W}_1^T\Gamma_1^{-1}\dot{\tilde{W}}_1\right]$$
$$={w_1}^T(x_2-\dot{y}_r+\Delta_1(\bar{x}_1,t))+tr\left[\tilde{W}_1^T\Gamma_1^{-1}\dot{\tilde{W}}_1\right]$$
$$={w_1}^T(x_{2d}+w_2+y_2-\dot{y}_r+\Delta_1(\bar{x}_1,t))$$
$$+tr\left[\tilde{W}_1^T\Gamma_1^{-1}\dot{\tilde{W}}_1\right]$$
$$\leq -k_1{w_1}^T w_1-\frac{1}{2}\eta_1 tr\left[\tilde{W}_1^T\tilde{W}_1\right]$$
$$+\frac{1}{2}\eta_1\left\|W^*\right\|_F^2+\varepsilon_{1H}+{w_1}^T w_2+w_1^T y_2$$

Then

$$\dot{V}_1\leq -\rho_1 V_1+{w_1}^T w_2+{w_1}^T y_2+C_1$$
$$\|w_1\|\leq\sqrt{2L(0)+\frac{2C}{\rho}},\ \|y_2\|\leq\sqrt{2L(0)+\frac{2C}{\rho}}$$
$$\dot{V}_1\leq -\rho_1 V_1+2\left(2L(0)+\frac{2C}{\rho}\right)+C_1$$
$$=-\rho_1 V_1+C_1' \tag{51}$$

So it can be inferred that:

$$\dot{V}=\sum_{i=1}^{3}\dot{V}_i=\sum_{i=1}^{3}(-\rho_i V_i+C_i')\leq -\rho V+C$$

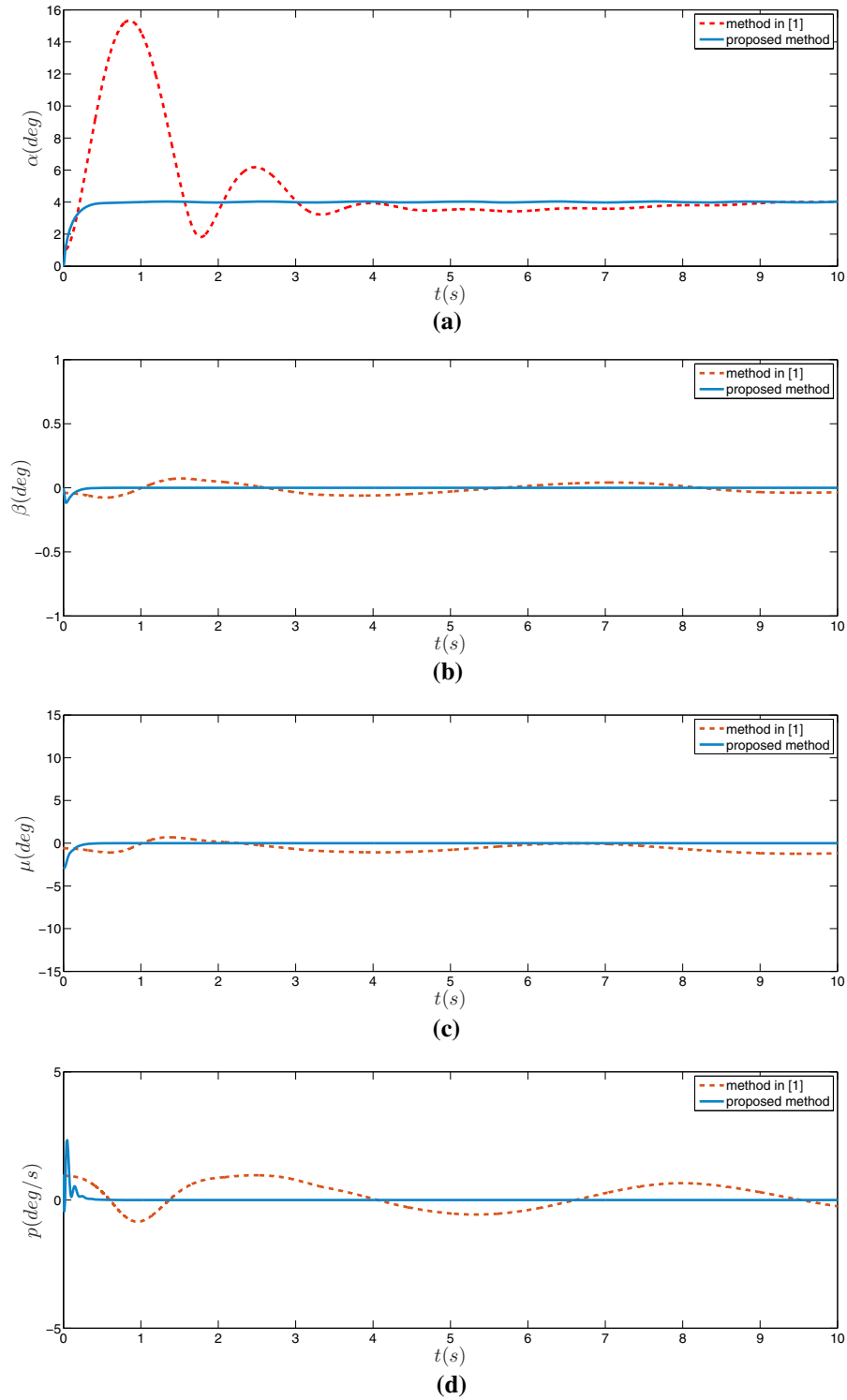

Fig. 2 Response curves of the NHV with different methods. **a** The attack angle α curve. **b** The sideslip angle β curve. **c** The bank angle μ curve. **d** The roll rate p curve. **e** The pitch rate q curve. **f** The yaw rate r curve

Fig. 2 continued

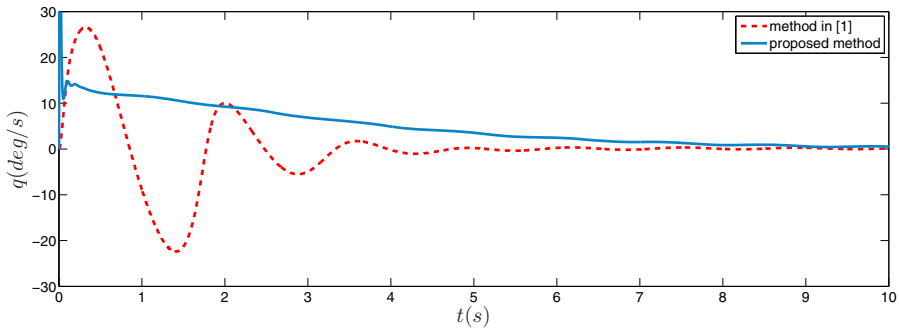

(e)

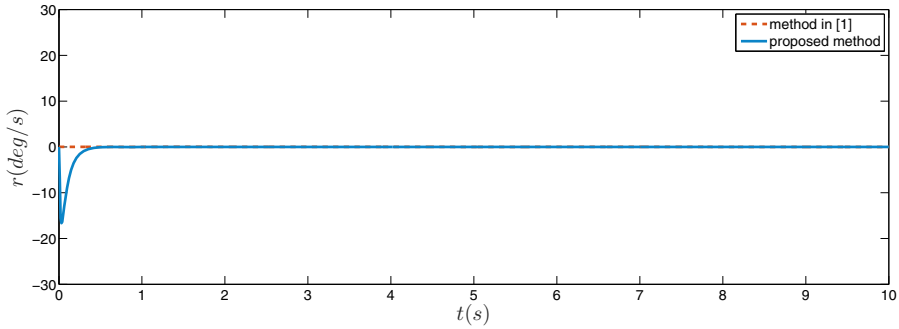

(f)

5 Simulation study

In this section, the proposed robust adaptive dynamic surface control strategy is applied to the NHV attitude dynamics model. Simulation results are presented to illustrate the effectiveness of the proposed robust control scheme. The initial conditions for the simulation of a near-space hypersonic vehicle are chosen as: $V_0 = 2100$ m/s, $H_0 = 27$ km, $\Delta V = 30$ m/s, $\Delta H = 60$ m, and $k_1 = k_2 = k_3 = 3$, $X = \left[V/10^4, H/10^5, V_c/10^4, H_c/10^5, \alpha, \gamma\right]^T$ is chosen as the input sample. The center of the Gaussian basis function is $b_1 = 4$, $b_2 = 3$, $b_3 = 2$, the width is $c_1 = [0.2; 0.3; 0.2; 0.3; 0.1; 0.1]$, $c_2 = [0.2; 0.3; 0.2; 0.3; 0.1; 0.1], c_3 = [2.1; 3; 2.1; 3; 0.1; 0.1]$, $\Gamma_1 = \text{diag}\,[10]$, $\Gamma_2 = \text{diag}\,[10]$, $\Gamma_3 = \text{diag}\,[8]$. The torque disturbance is $1 \times 10^5 \cdot [\sin(5t), \sin(5t), \sin(5t)]^T$ N m.

The robust adaptive dynamic surface scheme was implemented for the NHV including disturbance and uncertainty characteristic typical of hypersonic conditions. The corresponding simulation results are shown in Figs. 1 and 2. Figure 1 shows the effect of both disturbance and non-disturbance. Attitude control converges rapidly to the desired flight attitude states without disturbance. A minor stochastic fluctuation occurs due to the effects of the disturbances. These results illustrate that the proposed approach has better robust performance. Figure 2 shows the response curves of the NHV with different methods. It is clear from Fig. 2 that the proposed control law makes the system stable, and the response of all three attitude angles track the desired objectives well. This figure also shows that the proposed adaptive dynamic surface approaches to the origin faster than the adaptive neural control scheme offered in [1]. The simulation results illustrate the effectiveness of the proposed method.

6 Conclusions

The backstepping control method based on a robust adaptive dynamic surface has been presented to address the convergence speed and performance of the NHV altitude control system. As the order of the longitudinal control system increases, the computational complexity increases. A RBFNN is used to approximate unknown nonlinear disturbances, and a robustness term is introduced in the virtual controller to eliminate the influence of composite interference on the system and to improve robustness and adaptability. The uniformly asymptotical convergence of all closed-loop signals

has been guaranteed by Lyapunov analysis. Satisfactory attitude tracking performance has been illustrated in simulations. DSC holds promise for NHV control applications and could also be used in other uncertain strict-feedback nonlinear systems in the presence of input saturation, output constraints, and unknown external disturbances.

Acknowledgements The authors are grateful to the Editor-in-Chief, the Associate Editor, and anonymous reviewers for their constructive comments based on which the presentation of this paper has been greatly improved. This work is partially supported by The Natural Science Foundation of Jiangsu Province (Granted No. BK20150246).

Appendix

The detailed expressions of the vectors W_1 and matrices Π_2, Ω_2 are:

$$W_1^T = \frac{1}{M}\begin{bmatrix} T_V\cos\alpha - D_V \\ -Mg\cos\gamma \\ -T\sin\alpha - D_\alpha \\ T_\lambda\cos\alpha \\ T_h\cos\alpha - D_h - Mg_h\sin\gamma \end{bmatrix} \tag{A-1}$$

$$\Omega_2 = \begin{bmatrix} w_{21} & w_{22} & w_{23} & w_{24} & w_{25} \end{bmatrix} \tag{A-2}$$

where

$$w_{21} = \begin{bmatrix} T_{VV}\cos\alpha - D_{VV} \\ 0 \\ -T_V\sin\alpha - D_{V\alpha} \\ T_{V\lambda}\cos\alpha \\ -D_{Vh} \end{bmatrix} \tag{A-3}$$

$$w_{22} = \begin{bmatrix} 0 & Mg\sin\gamma & 0 & 0 & -g_h\cos\gamma \end{bmatrix}^T \tag{A-4}$$

$$w_{23} = \begin{bmatrix} -T_V\sin\alpha - D_{\alpha V} \\ 0 \\ -T\cos\alpha - D_{\alpha\alpha} \\ -T_\lambda\sin\alpha \\ -T_h\sin\alpha - D_{\alpha h} \end{bmatrix} \tag{A-5}$$

$$w_{24} = \begin{bmatrix} T_{\lambda V}\cos\alpha & 0 & -T_\lambda\sin\alpha & T_{\lambda\lambda}\cos\alpha & 0 \end{bmatrix}^T \tag{A-6}$$

$$w_{25} = \begin{bmatrix} T_{hV}\cos\alpha - D_{hV} \\ -Mg_h\cos\gamma \\ -T_h\sin\alpha - D_{h\alpha} \\ T_{h\lambda}\cos\alpha \\ T_{hh}\cos\alpha - D_{hh} - Mg_{hh}\sin\gamma \end{bmatrix} \tag{A-7}$$

$$\pi_1 = \begin{bmatrix} \pi_{11} & \pi_{12} & \pi_{13} & \pi_{14} & \pi_{15} \end{bmatrix}^T \tag{A-8}$$

where

$$\pi_{11} = \frac{(L_V + T_V\sin\alpha)V - (L + T\sin\alpha)}{MV^2} + \frac{g\cos\gamma}{V^2} \tag{A-9}$$

$$\pi_{12} = \frac{g\sin\gamma}{V} \tag{A-10}$$

$$\pi_{13} = \frac{L_\alpha + T\cos\alpha}{MV} \tag{A-11}$$

$$\pi_{14} = \frac{T_\lambda\sin\alpha}{MV} \tag{A-12}$$

$$\pi_{15} = \frac{L_h + T_h\sin\alpha}{MV} - \frac{g_h\cos\gamma}{V} \tag{A-13}$$

$$\Pi_2 = \begin{bmatrix} \pi_{21} & \pi_{22} & \pi_{23} & \pi_{24} & \pi_{25} \end{bmatrix} \tag{A-14}$$

where

$$\pi_{21} = \begin{bmatrix} \frac{(L_{VV}+T_{VV}\sin\alpha)}{MV} - \frac{2(L_V+T_V\sin\alpha)}{MV^2} + \frac{2(L+T\sin\alpha)}{MV^3} - \frac{2g\cos\gamma}{V^3} \\ -\frac{g\sin\gamma}{V^2} \\ \frac{L_{V\alpha}+T_V\cos\alpha}{MV} - \frac{L_\alpha+T\cos\alpha}{MV^2} \\ \frac{T_{V\lambda}\sin\alpha}{MV} - \frac{T_\lambda\sin\alpha}{MV^2} \\ \frac{L_{Vh}+T_{Vh}\sin\alpha}{MV} - \frac{L_h+T_h\sin\alpha}{MV^2} + \frac{g_h\cos\gamma}{V^2} \end{bmatrix} \tag{A-15}$$

$$\pi_{22} = \begin{bmatrix} -\frac{g\sin\gamma}{V^2} & \frac{g\cos\gamma}{V} & 0 & 0 & \frac{g_h\sin\gamma}{V} \end{bmatrix}^T \tag{A-16}$$

$$\pi_{23} = \begin{bmatrix} \frac{L_{\alpha V}+T_V\cos\alpha}{MV} - \frac{L_\alpha+T\cos\alpha}{MV^2} \\ 0 \\ \frac{L_{\alpha\alpha}-T\sin\alpha}{MV} \\ \frac{T_\lambda\cos\alpha}{MV} \\ \frac{L_{\alpha h}+T_h\cos\alpha}{MV} \end{bmatrix} \tag{A-17}$$

$$\pi_{24} = \begin{bmatrix} \frac{T_{\lambda V}\sin\alpha}{MV} - \frac{T_\lambda\sin\alpha}{MV^2} \\ 0 \\ \frac{T_\lambda\cos\alpha}{MV} \\ \frac{T_{\lambda\lambda}\sin\alpha}{MV} \\ \frac{T_{\lambda h}\sin\alpha}{MV} \end{bmatrix} \tag{A-18}$$

$$\pi_{25} = \begin{bmatrix} \frac{L_{hV}+T_{hV}\sin\alpha}{MV} - \frac{L_h+T_h\sin\alpha}{MV^2} + \frac{g_h\cos\gamma}{V^2} \\ \frac{g_h\sin\gamma}{V} \\ \frac{L_{h\alpha}+T_{h\alpha}\sin\alpha+T\cos\alpha}{MV} \\ \frac{T_{h\lambda}\sin\alpha}{MV} \\ \frac{L_{hh}+T_{hh}\sin\alpha}{MV} - \frac{g_{hh}\cos\gamma}{V} \end{bmatrix} \tag{A-19}$$

References

1. Yan, X., Chen, M., Wu, Q., Shao, S.: Adaptive neural tracking control for near-space vehicle with stochastic disturbances. Int. J. Adv. Robot. Syst. **14**(3), 1–10 (2017)
2. Alsuwian, T.: Comparison of PID and nonlinear feedback linearization controls for longitudinal dynamics of hypersonic vehicle at subsonic speeds. In: Proceedings of the IEEE National Aero-space Electronics Conference, NAECON, 207-213, February 14 (2017)
3. Sagliano, M., Mooij, E., Theil, S.: Adaptive disturbance-based high-order sliding-mode control for hypersonic-entry vehicles. J. Guid. Control Dyn. **40**(3), 521–536 (2017)
4. Wiese, D.P., Annaswamy, A.M., Muse, J.A., Bolender, M.A., Lavretsky, E.: Adaptive output feedback based on closed-loop reference models for hypersonic vehicles. J. Guid. Control Dyn. **38**(12), 2429–2440 (2015)
5. Lamorte, N., Friedmann, P.P., Dalle, D.J., Torrez, S.M., Driscoll, J.F.: Uncertainty propagation in integrated airframeC propulsion system analysis for hypersonic vehicles source. J. Propulsi. Power **31**(1), 54–68 (2015)
6. Sziroczak, D., Smith, H.: A review of design issues specific to hypersonic flight vehicles source. Prog. Aerosp. Sci. **84**, 1–28 (2016)
7. Starkey, R.P.: Hypersonic vehicle telemetry blackout analysis source. J. Spacecr. Rockets **52**(2), 426–438 (2015)
8. Keith C.: DARPA HTV-2 Second Test Flight Report Released. http://spaceref.com/aeronautics/darpa-htv-2-second-testflight-report-released.html. cited 22 April 2012
9. Qi, C., Jianliang, A.: NDI-based L1 adaptive control design for a generic hypersonic vehicle model. In: AIAA Guidance, Navigation, and Control Conference, Texas, pp. 1–17 (2017)
10. Mobayen, S., Baleanu, D., Tchier, F.: Second-order fast terminal sliding mode control design based on LMI for a class of non-linear uncertain systems and its application to chaotic systems. J. Vib. Control. **23**(18), 2912–2925 (2017)
11. He, N.B., Gutierrez, H., Gao, Q., Jiang, C.S.: Fuzzy terminal slide-mode control for hypersonic vehicle. J. Intell. Fuzzy Syst. **33**, 1831–1839 (2017)
12. Xu, H.J., Mirmirani, M.D., Ioannou, P.A.: Adaptive sliding mode control design for a hyper-sonic flight vehicle. J. Guid. Control Dyn. **27**, 829–838 (2004)
13. Chen, M., Jing, Y.: Adaptive dynamic surface control of NSVs with input saturation using a disturbance observer. Chin. J. Aeronaut. **28**(3), 853–864 (2015)
14. Chen, M., Jiang, C.-S., Wu, Q.-X.: Disturbance-observer-based robust flightcontrol for hypersonic vehicles using neural networks. Adv. Sci. Lett. **4**, 1771–1775 (2011)
15. Jiang, B., Zhang, K., Shi, P.: Integrated fault estimation and accommodation design for discrete-time Takagi–Sugeno fuzzy systems with actuator faults. IEEE Trans. Fuzzy Syst. **19**(2), 291–304 (2011)
16. Fu, J., Wu, Q.X., Jiang, C.S., Cheng, L.: Robust sliding mode control with unidirectional auxiliary surfaces for a nonlinear with state constraints. Control Decis. **26**(9), 1288–1294 (2011)
17. Pu, M., Wu, Q.-X., Jiang, C.-S., Cheng, L.: Application of adaptive second-order dynamic terminal sliding mode control to near space vehicle. J. Aerosp. Power **25**(5), 1169–1176 (2010)
18. Du, Y.L., Wu, Q.X., Jiang, C.S., Wen, J.: Adaptive functional link network control of near-space vehicles with dynamical uncertainties. J. Syst. Eng. Electron. **21**(5), 868–876 (2010)
19. Wang, Y.H., Wu, Q.X., Jiang, C.S.: Reentry attitude tracking control based on fuzzy feed-forward for reusable launch vehicle. Int. J. Control Autom. Syst. **7**(4), 503–511 (2009)
20. Gao, G., Wang, J.Z.: Reference command tracking control for an air-breathing hypersonic vehicle with parametric uncertainties. J. Frank. Inst **350**(5), 1155–1188 (2013)
21. Mobayen, S., Baleanu, D.: Stability analysis and controller controller design for the performance improvement of disturbed nonlinear systems using adaptive global sliding mode control approach. Nonlinear Dyn. **83**(3), 1557–1665 (2016)
22. Mobayen, S., Tchier, F.: Design of an adaptive chattering avoidance global sliding mode tracker for uncertain nonlinear time-varying systems. Trans. Inst. Meas. Control. **39**(10), 1547–1558 (2017)
23. Mobayen, S., Tchier, F., Ragoub, L.: Design of an adaptive tracker for n-link rigid robotic manipulators based on super-twisting global nonlinear sliding mode control. Int. J. Syst. Sci. **48**(9), 1990–2002 (2017)
24. Huang, P., Dongke, W., Meng, Z., Zhang, F.: Adaptive post-capture backstepping control for tumbling tethered space robotCtarget combination. J. Guid. Control Dyn. **39**(1), 150C156 (2016)
25. Xia, G.: Adaptive neural network control with backstepping for surface ships with input dead-zone. Math. Probl. Eng. **2013**, 1–9 (2013)
26. Sun, L.-Y., Tong, S., Liu, Y.: Adaptive backstepping sliding mode control of static var compensator. IEEE Trans. Control Syst. Technol. **19**(5), 1178–1185 (2011)
27. Jiang, C., Wu, Q., Fei, S.: Modern Nonlinear Robust Control System M. Harbin Institute of Technology Press, Harbin (2012)
28. Khalil, H.K.: Nonlinear Control M. Prentice-Hall, New Jersey (1996)
29. Cheng, C.-C., Chiang, Y.-C., Huang, P.-C.: Design of adaptive block back-stepping controllers with perturbations estimation for nonlinear state-delayed systems in semi-strict feedback form. Asian J. Control **19**(3), 856–873 (2017)
30. Wang, D., Huang, J.: Neural network-based adaptive dynamic surface control for a class of uncertain nonlinear systems in strict-feedback form. IEEE Trans. Neural Netw. **16**(1), 195–202 (2005)
31. Yu, Z.X., Lin, Y.: A robust adaptive dynamic surface control for nonlinear systems with hysteresis Input. Acta Autom. Sin. **36**(9), 1264–1271 (2010)